Check for updates

DOI: 10.1002/((please add manuscript number))

Article type: Communication

Tailor-Made Microporous Metal-Organic Frameworks for the Full Separation of Propane from Propylene Through Selective Size Exclusion

*Hao Wang, Xinglong Dong, Valentina Colombo, Qining Wang, Yanyao Liu, Wei Liu, Xin-Long Wang, Xiao-Ying Huang, Davide M. Proserpio, Angelo Sironi, Yu Han, and Jing Li**

Dr. H. Wang, Q.N. Wang, Y.Y. Liu, Prof. J. Li

Department of Chemistry and Chemical Biology

Rutgers University

610 Taylor Road, Piscataway, NJ, 08854, USA

Email: jingli@rutgers.edu

Dr. X.L. Dong, Prof. Y. Han

Advanced Membranes and Porous Materials Center

Physical Sciences and Engineering Division

King Abdullah University of Science and Technology

Thuwal 23955-6900, Kingdom of Saudi Arabia

Dr. V. Colombo, Prof. D.M. Proserpio, Prof. A. Sironi

Dipartimento di Chimica

Università degli Studi di Milano

20133 Milano, Italy

This is the author manuscript accepted for publication and has undergone full peer review but has not been through the copyediting, typesetting, pagination and proofreading process, which may lead to differences between this version and the Version of Record. Please cite this article as doi: 10.1002/adma.201805088.

This article is protected by copyright. All rights reserved.

Author Manuscript

Prof. X.-L. Wang

Department of Chemistry

Northeast Normal University

Changchun 130024, Jilin, China

Prof. X.-Y. Huang

State Key Laboratory of Structural Chemistry

Fujian Institute of Research on the Structure of Matter

the Chinese Academy of Sciences Fuzhou

Fujian, 350002, P.R. China

Dr. H. Wang, Dr. W. Liu, Prof. J. Li

Hoffmann Institute of Advanced Materials

Shenzhen Polytechnic

Xili, Nanshan, Shenzhen 518055, China

Prof. D.M. Proserpio

Samara Center for Theoretical Materials Science (SCTMS)

Samara State Technical University

Samara 443100, Russia

Keywords: metal-organic frameworks, adsorbent, adsorptive separation, olefin/paraffin separation, molecular sieving

Abstract: Adsorptive separation of olefin/paraffin mixtures by porous solids could greatly reduce the energy consumption associated with the currently employed cryogenic distillation technique. Here we report the complete separation of propane and propylene by a designer microporous metal-organic framework (MOF) material. The compound, $Y_6(OH)_8(abtc)_3(H_2O)_6(DMA)_2$ (Y-abtc, abtc = 3,3',5,5'-azobenzene-tetracarboxylates, DMA = dimethylammonium), is rationally designed through topology-guided replacement of inorganic building units. Y-abtc is both thermally and hydrothermally robust, and possesses optimal pore window size for propane/propylene separation. It adsorbs propylene with fast kinetics under ambient temperature and pressure, but fully excludes propane, as a result of selective size exclusion. Multicomponent column breakthrough experiments confirm polymer-grade

This article is protected by copyright. All rights reserved.

Author Manuscript

propylene (99.5%) can be obtained by this process, demonstrating its true potential as an alternative sorbent for efficient separation of propane/propylene mixtures.

Olefin/Paraffin separation, listed among the "seven chemical separations to change the world",[1] is of high commercial importance as highly pure olefins (e.g. propylene and ethylene) are required to comply "polymer-grade" specifications for the manufacture of plastics. The separation is, however, particularly difficult to accomplish because of the close volatilities of the components.[2] Propylene is one of the most important olefins in petrochemical industry, primarily because of its use in the production of polypropylene, the world's second-most widely produced synthetic plastic. The global demand for polypropylene has been rising continuously and its annual growth rate is expected to be 4-5% before 2020, resulting in increasing need for polymer-grade (> 99.5 %) propylene.[3] Nevertheless, the production of highly pure propylene represents a challenging and complicated process, which involves the separation of propylene from a propane/propylene mixture. Propane/propylene mixtures are typically obtained by steam cracking of naphtha or during fluid catalytic cracking of gas oils in refineries, with a propylene purity of 50-60% for the former and 80-87% for the latter. Conventional separation of propane and propylene relies on cryogenic distillation, which is carried out at about 243 K and 0.3 MPa in a column containing over 100 trays.[4] Undoubtedly, this heat-driven process is highly energy-intensive.

To lower the energy and operational cost and to suppress the carbon emissions associated with the propylene purification process through cryogenic distillation, several alternative technologies have been proposed and among them, adsorptive separation, such as pressure/temperature swing adsorption and gas phase simulated moving bed have demonstrated great promise and can potentially offer higher energy efficiency.[3] In this context, the development of a suitable adsorbent is of paramount importance for successful implementation of the adsorptive separation technology. To this end, a wide variety of porous solids have been examined for the separation of propane and propylene, including silica-gel,[5] zeolites,[6-7] and carbon molecular sieves[8] to name a few. However, these materials have yet to meet the stringent requirement for industrial implementation, and thus, search for ideal adsorbents remains ongoing.

The newly emerged family of crystalline sorbent materials, metal-organic frameworks (MOFs),[9-12] hold particular promise for hydrocarbon separation including paraffin/olefin separation in light of their tunable pore size, pore shape, and surface functionality.[13-17] Long and coworkers demonstrated that MOFs with open metal sites show favorable adsorption toward olefins over paraffins as a result of a side-on coordination of olefins at the unsaturated metal centers.[18-19] Thus, this type of MOF materials, analogous to π-complexation zeolites/mesoporous silica,[20-21] are capable of discriminating multiple olefins (e.g. ethylene + propylene) from paraffins through thermodynamically-driven separation. On the other hand, in the case of propane/propylene separation, where the removal of a single olefin from its corresponding paraffin is needed, kinetically-driven separation often proves to be more suitable and efficient.[3] A number of adsorbents have been reported to undergo kinetic separation toward propane and propylene.[22-24] Compared to conventional adsorbents, the MOF pore size can be tuned much more readily to achieve significantly improved performance for kinetic separation of the two C3 molecules, as demonstrated in several recent studies.[15, 24] The third separation mechanism is based on selective size exclusion where one adsorbate is adsorbed while the other is completely excluded. This mechanism is considered an ideal scenario for gas separation as it offers the highest separation selectivity among three different mechanisms.[15, 25] A widely studied example is Zeolite 4A[26-27] as it selectively adsorbs propylene but excludes propane. However, its adsorption kinetics for propylene is very slow, resulting in poor separation performance under mixed-gas conditions.[15]

This article is protected by copyright. All rights reserved.

Herein, we show that Y-abtc, a microporous metal-organic framework material with cage-like pores, exhibits fast and complete separation of propane/propylene mixtures through selective molecular exclusion mechanism. The optimal pore structure of this material is achieved by a topology-guided design strategy, which involves the precise tuning of pore aperture by judicious selection of structure topology, inorganic nodes and organic linkers. Like zeolite 4A, Y-abtc adsorbs propylene but fully excludes propane, yet it is superior to zeolite 4A as it exhibits a much faster adsorption kinetics for propylene. Multicomponent column breakthrough measurements demonstrate that Y-abtc is capable of producing propylene with a purity of 99.5% from a typical mixture concentration of cracking product, meeting the "polymer grade" specification required for the production of polypropylene. This structure, built on hexanuclear Y6 clusters, exhibits high thermal and hydrothermal stability. In addition, its synthesis is facile and can be easily scaled up. It should be noted that during the preparation of this manuscript, Eddaoudi et al. reported a similar structure built on Tb and abtc, which shows kinetic separation rather than selective size exclusion toward propane and propylene.[28] In light of its attractive structural features, fast adsorption kinetics and highest selectivity for propylene over propane, we believe Y-abtc represents a notable advancement for the adsorptive separation of the C3 paraffin and olefin, and holds strong promise for industrial implementation. Furthermore, the material design strategy presented here may offer guidance for further research and advancement in developing MOFs with suitable pore structure for industrially challenging molecular separations.

We recently reported topology-guided construction of Zr-MOFs built on tetratopic carboxylate linkers and their uses for the separation of C6 alkane isomers.[29] As Zr_6O_8 building block is commonly adopted in Zr-MOFs, their structural topology, depending on the connectivity of the Zr6 cluster and the geometry of the organic linker, is generally predictable or designable by making use of reticular chemistry. Three different structures with **ftw**, **scu**, and **lvt** topology were obtained and the connectivity of the Zr6 cluster and the topology of the resulting Zr-MOFs are closely related to the shape (i.e. aspect ratio) of the organic linker. The use of the smallest linker bptc led to the formation of a **ftw** type structure with 12-connected Zr6 cluster (Zr-bptc). Structures with **ftw** topology are particularly favorable for molecular separation as they feature large cages connected through small windows.[30] The pore aperture is mainly regulated by the size of the organic linker (i.e. distance between adjacent carboxylates). Zr-bptc shows optimal pore aperture for the separation of alkane isomers as it adsorbs linear alkanes only and excludes any branched isomers. With this in mind, it is reasonable to speculate that a similar structure with slightly reduced size of pore window may be suitable for discriminating linear paraffins and olefins such as propane and propylene. However, in practice, this is difficult to achieve by replacing bptc with an even shorter ligand. This is because bptc, comprised of two isophthalates, may be the smallest organic linker suited for the construction of **ftw** type structure. An alternative approach is to explore the possibility of modifying the inorganic building unit while maintaining the overall connectivity and topology. A careful screening analysis suggests that Y6 cluster, which resembles the Zr6 cluster with respect to composition, geometry, and connectivity, may be a good choice.[31-32] Reported by Eddaoudi and coworkers,[33] Y6 cluster connects to carboxylate linkers in a similar fashion as that of Zr6 in Zr-MOFs, and forms structures with identical topology to that of the latter with the same organic linkers (**Figure 1**). Nevertheless, due to the negative charge of the 12-connected cluster $[Y_6(OH)_8(H_2O)_6(COO)_{12}]^{2-}$ and the propagated framework, balancing cations (usually dimethylammonium, assuming N,N-dimethylformamide is the solvent used for synthesis) are present in the structure, which can potentially act as a regulatory factor to fine control and adjust pore dimensions.[34] For a given organic linker, the presence of charge balancing cations in the Y6 based MOF may slightly reduce the effective pore size compared to its analogous structure built on Zr6 cluster. This prompted us to explore the possibility of replacing Zr6 clusters in the aforementioned Zr-MOFs by Y6 cluster, thus fine-tuning the pore size of MOFs for the separation of propane and propylene.

This article is protected by copyright. All rights reserved.

Author Manuscript

Our initial attempt started with the synthesis of Y-MOF with H_4bptc, aiming at a **ftw** structure analogous to Zr-bptc but with slightly smaller pore aperture in hope that the resultant structure may be suitable for the target separation of propane and propylene. Colorless cubic crystals of Y-bptc was successfully obtained via solvothermal reactions of $Y(NO_3)_3 \cdot 6H_2O$ and H_4bptc in a mixed solvent of DMF and water, using 2-fluorobenzoic acid as an acidic modulator (Figure S1).[35] Single crystal X-ray diffraction analysis reveals that Y-bptc crystallizes in the cubic *Im-3* space group. As expected, the structure is built on 12-connected $[Y_6(OH)_8(H_2O)_6(COO)_{12}]^{2-}$ SBU with six Y^{3+} ions assembled into an octahedron where μ_3-OH^- anions occupy the eight facets of the octahedron (Figure S2). Each Y^{3+} ion is nine coordinated, connecting to four oxygen atoms from four different carboxylate groups, four bridging μ_3-OH^- anions, and one terminal water molecule. The inorganic cluster is slightly different from the commonly observed 12-connected $Zr_6O_4(OH)_4(COO)_{12}$. Due to the lower positive charge of Y^{3+} compared to Zr^{4+}, the four bridging μ_3-O^{2-} in Zr-MOFs are replaced by μ_3-OH^- in Y-analogues. The Y6 cluster is negatively charged while the Zr6 cluster is neutral. In addition, each Y^{3+} is coordinated to an additional terminal water, which is not observed for Zr-based structures. Despite of these differences, the overall connectivity of Y-bptc is identical to that of Zr-bptc, forming the expected **ftw** type structure. Thus it also contains cubic cage-like pores with Y6 clusters on the vertices and $bptc^{4-}$ linkers on the faces, and the cages are interconnected through small windows (**Figure 1**). While preparing this manuscript we noted a report of the same structure appeared very recently.[28] The phase purity of Y-bptc was confirmed by powder X-ray diffraction analysis (Figure S3).

As will be explained in the following sections, while we demonstrate the pore size of Y-bptc can indeed be effectively reduced with respect to Zr-bptc as a result of topology-directed SBU replacement, such reduction is overly done making the pore window too small to adsorb either propane or propylene. Thus we attempted to further tune the pore size by using a slightly longer organic linker 3,3′,5,5′-azobenzene-tetracarboxylate (H_4abtc) with the Y6 SBU. Solvothermal reactions of $Y(NO_3)_3 \cdot 6H_2O$ and H_4abtc under conditions similar to that of Y-bptc yielded light-yellow, small, block-shaped crystals (Figure S1). Although powder X-ray diffraction patterns indicated its high crystallinity (Figure S4), attempts for determining the structure by single crystal X-ray diffraction analysis didn't succeed. We instead decided to try to retrieve the crystal structure through *ab initio* structure solution methods (See Supporting Information for details).[36-37] Indexing of the powder pattern suggested that Y-abtc, differently from Y-bptc, crystallizes in a rhombohedal rather than a cubic space group. This was eventually confirmed by a successful structure solution (R_p, R_{wp} and R_{Bragg} = 0.0754, 0.1022 and 2.218, respectively, Figure S5) in the *R-3c* space group. The overall connectivity of Y-abtc is identical to that of Y-bptc (**Figure 2**). However, the cages are no longer cubic, because of the rotation of the octahedron driven by the connectivity of the different ligands (Figure S6). As a result, for each face of the cube, in Y-bptc, the plane described by the 4 center of mass of the octahedrons and the one described by the ligand are coincident. For Y-abtc, however, the two planes are not any more coincident and this is due to 1) the mutual rotation of the octahedrons and 2) the coordination geometry of the ligand. The ligand coordination is indeed straight on the Y atom for two COO^- groups and above and below from this plane by the other two COO^- groups (Figure S7). This gives rise to the contraction and distortion of the cage. It should be noted that Y-abtc adopts a 4,12-c connectivity, which is different from Zr-abtc with 4,8-c connectivity as a result of the large aspect ratio of $abtc^{4-}$ (**Figure 1**).[29] A recent paper by an IUPAC committee[38] explains the different approaches in the deconstruction of crystalline networks into underlying nets, showing how to deal with structures with polytopic ligands and complex SBUs like our compounds. In the commonly used description[38] ("single node" deconstruction) the SBU is a 12-coordinated node and the ligand 4-c (regardless of the shape) resulting in the 4,12-c **ftw** underlying net. If we use the "all node" deconstruction[37] (called "cluster" in ToposPro) we describe the tetratopic ligand as formed by two 3-c nodes. This allows to consider the shape and orientation of ligand on the underlying net giving three 3,12-c nets derived from 4,12-**ftw**: **ttv**, **kle** and **kxe.**[36] Until recently only

This article is protected by copyright. All rights reserved.

3,12-**kle** was observed for ligand of rectangular shape and symmetry D_{2h}[29] and now also for Y-bptc. The change of the ligand to abtc (lowering the symmetry to C_{2h}) in Y-abtc gave access to the new topology 3,12-**kxe** that differs from 3,12-**kle** for the relative orientations of the ligands as shown in the Figure S8. In the Y-abtc crystal structure the clathrate solvent molecules and the balancing extra-framework cations are disordered into the voids of this MOF. We manage to partly eliminate the solvent by a thermal treatment (see Supplementary Information for details) thus reducing the diffuse electron density in the pores but also increasing the disorder by leaving more 'free room' for the cations and the residual solvent. We estimate that the effect of our description of the diffuse electron density in the 'pores' has the same order of magnitude of the intrinsic inaccuracy of powder data and has little effect on the stereochemistry of the organic-inorganic framework. Indeed, the comparison with the Tb-abtc structure, with which we came across after having solved the Y-abtc structure, confirms that *ab initio* structure solution from powder diffraction data is a truly powerful tool, since the two structural models strongly agrees.

Porosity characterization by N_2 adsorption at 77 K didn't work out for Y-bptc or Y-abtc as neither of them show noticeable uptake of N_2 (Figure S9). This is different from their Zr-based analogues (Zr-bptc and Zr-abtc) which adsorb substantial amount of N_2 at 77 K. A possible reason could be the existence of balancing cations in the Y-based structures, leading to the suppression of accessible size of pore windows which does not allow the diffusion of N_2 into their pores at cryogenic temperature. We then turned to characterize their porosity by CO_2 adsorption at 195 K. Y-bptc and Y-abtc both exhibit Type I adsorption profile for CO_2, with saturation capacities of 3.2 and 3.7 mmol g^{-1}, respectively. The estimated surface areas and pore volumes are 319 and 427 m^2 g^{-1}, and 0.14 and 0.18 cc g^{-1} for Y-bptc and Y-abtc, respectively. These values are noticeably lower than their Zr-based analogues.[29]

Adsorption isotherms of propane and propylene on Zr-bptc and Zr-abtc at room temperature indicate neither of them is capable of discriminating the two gases (**Figure 3**a and **3**b). The adsorption capacity of propane and propylene are similar for both compounds. Besides, no diffusional restriction has been observed. The results suggest that the aperture sizes of Zr-bptc and Zr-abtc are too large for the separation of propane and propylene. In contrast, while Y-bptc features the same connectivity and topology as Zr-bptc, it adsorbs neither propane nor propylene, indicating its pore aperture size is smaller than that of Zr-bptc (**Figure 3**c). This could be attributed to the existence of the balancing cation, dimethylammonium, which might block the entrance of the cage and suppress the effective pore aperture. A more detailed discussion will be presented in the following section.

Unlike Y-bptc, Y-abtc adsorbs appreciable amount of propylene at room temperature, with an uptake capacity of ~ 2 mmol g^{-1} at 1 bar (**Figure 3**d). The adsorption is fully reversible and features a Type I profile. Adsorption isotherms at higher temperatures (40, 60, 80 °C) have also been collected, and at 80 °C propylene adsorption capacity is ~ 1.5 mmol g^{-1} (**Figure 3**e). Adsorption strength has been evaluated by isosteric heat of adsorption (Q_{st}), calculated by adsorption isotherms at 40, 60, and 80 °C and a Q_{st} value of ~50 kJ mol^{-1} was obtained. This value is comparable to M_2(dobdc) (M = Mg, Mn, Fe, Co, Ni, Zn), but slightly lower than that of KAUST-7 (57.4 kJ mol^{-1}).[15, 18] We believe the relatively high adsorption heat of Y-abtc for propylene is a combined effect of pore confinement and strong interaction at the charge-balancing cationbinding sites. The pore aperture size of Y-abtc (4.72 Å, Figure 6d) matches very well with the kinetic diameter of propylene (4.68 Å), which leads to strong pore confinement effect. This was also observed in the case of KAUST-7 which has a Q_{st} for propylene as high as 57.4 kJ mol^{-1}, as a result of the perfect match between the MOF aperture size and the size of propylene.[15] In addition, the charge-balancing cation dimethylammonium may also contribute to the high adsorption affinity, making the Q_{st} value higher than MOFs with open metal sites.[18] The cation effect has been commonly observed in cation exchanged zeolites,[39] as well as in

This article is protected by copyright. All rights reserved.

Tb-abtc which has an adsorption heat of 48.8 kJ/mol obtained from calorimetric measurement. The value agrees well with ours.[28] In contrast, adsorption isotherm at room temperature shows essentially no uptake of propane on Y-abtc, indicating a size-exclusion behavior. To confirm the discrimination toward propane and propylene by Y-abtc is through selective size exclusion rather than kinetic separation and to assess the adsorption kinetics of propylene, adsorption rates of propane and propylene at 25 °C and 80 °C were measured with a gravimetric adsorption analyzer (see Supporting Information for details). As shown in **Figure 3**f, adsorption of propylene reaches equilibrium within 20 and 10 minutes at 25 and 80 °C, respectively, without noticeable diffusional restrictions. On the contrary, negligible uptake of propane has been detected and it shows no difference with respect to adsorption kinetics at 25 and 80 °C. This is consistent with the adsorption isotherms, indicating propane is fully excluded from diffusing into the pore of Y-abtc. These results suggest that Y-abtc represents a rare adsorbent that exhibits selective molecular exclusion behavior for propane over propylene. Such a property of Y-abtc can be attributed to its optimal pore window size (4.72 Å, Figure 6d) which falls between the kinetic diameter of propylene (4.68 Å) and propane (5.1 Å).[40]

To assess the framework robustness of Y-abtc with respect to crystallinity and adsorption performance, stability test was performed with thermal and hydrothermal treatments. *In situ* variable-temperature PXRD analysis shows that the framework remains intact up to 520 °C, temperature at which loss of crystallinity starts to take place (Figure S10). Le Bail refinement and parametric treatment of the VT-PXRD data along the whole range of temperature (RT - 540 °C) shows that during activation the framework undergoes a slight contraction of the unit cell volume of less than 1 % (Figure S11). This result displays that Y-abtc possesses high framework robustness, similar to its Zr-based analogues (Zr-bptc and Zr-abtc). As shown in **Figure 4**, after being heated at 180 °C in open air or in water at 80 °C for 3 days, the crystallinity of Y-abtc was well maintained, as evidenced by the PXRD patterns collected on the samples after treatments. More importantly, their propylene adsorption capacity was also fully retained (**Figure 4**b).

As suggested by the single component adsorption results, Y-abtc exhibits potential of separating propane and propylene through complete sieving. We thus performed multicomponent column breakthrough experiments at room temperature to assess its separation capability under mixed gases conditions. We started with an equimolar binary mixture of propane and propylene and a total flow rate of 1.6 ml min^{-1} as a feed. The breakthrough curve reveals that propane breaks at the very first minute indicating no noticeable retention took place in the column (**Figure 5**a). This is consistent with the single component adsorption result that Y-abtc does not adsorb propane at room temperature. Conversely, propylene, the other component in the mixture does not elute out until the 12^{th} minute, equivalent to a dynamic uptake of 1.26 mmol g^{-1}. This again, coincides with the pure component adsorption results that propylene can freely diffuse into the pore of Y-abtc. Subsequent desorption of the gas retained in the column by heating under helium flow yielded a propylene purity of 97.6 % in the eluted gas (**Figure 5**b). A following breakthrough experiment with an increased flow rate (total flow rate: 4 ml min^{-1}) confirmed the complete separation capability of Y-abtc was fully retained with a retention time of 12.9 minutes per gram of adsorbent for propylene (Figure S12), a value noticeably higher than that of KAUST-7, the MOF material with the best performance reported so far for propane/propylene separation, which has a retention time of 5.7 minutes per gram of adsorbent under the same condition.[15] This indicates the dynamic adsorption capacity of Y-abtc for propylene is more than twice higher than that of KAUST-7. This is a significant improvement considering its complete sieving nature for the propane/propylene separation, scalable synthesis （Figure S13 and S14）and high stability.

Author Manuscript

This article is protected by copyright. All rights reserved.

Separation of propane and propylene by cryogenic distillation is particularly energy intensive as the production of polymer-grade propylene with a purity of 99.5% requires distillation tower that contains a large number of theoretical plates and is operated with large reflux/feed ratios with tremendous energy input. Thus production of highly pure propylene by adsorptive separation could largely lower the energy cost associated with the separation process.[3] In this context, we further explored the breakthrough experiments with different propane/propylene starting ratios, i.e. propane:propylene = 10:90, and propane:propylene = 5:95 (Figure S12). Clear separation of propane and propylene with propane breaking first was observed in the breakthrough curves for both feed ratios despite the increase of the concentration of propylene in the mixture. For the measurement starting with a mixture of propane: propylene = 5:95, although propane was also retained in the column for several minutes before breaking due to its low concentration, its adsorbed amount on Y-abtc (~ 2 mg g^{-1}) is negligible (**Figure 5**c). Noticeably, 99.5% pure propylene was recovered during the desorption step, a purity that well meets the requirements for the production of polymers (**Figure 5**d). This confirms that Y-abtc, as an adsorbent for complete sieving of propane from propylene, is capable of producing polymer-grade propylene by adsorptive separation method. As mentioned previously, the recently reported Tb-abtc was also examined for the adsorptive separation of propane and propylene. It adsorbs similar amount of propane and propylene at room temperature but the adsorption kinetics for propane is significantly slower than that of propylene, enabling kinetic-based separation of the two gases by mixed-gas breakthrough experiments.[28] In this work the separation is achieved via a different and more efficient mechanism, namely size exclusion. Y-abtc adsorbs propylene and fully excludes propane. The higher selectivity associated with this mechanism is likely the reason for the higher dynamic adsorption capacity of Y-abtc (1.26 mmol g^{-1}) than that of Tb-abtc (0.9 mmol g^{-1}) under similar conditions (room temperature and with a feed of C_3H_8/C_3H_6:50/50).

The 4,12-c Y-abtc/Y-bptc are similar to their Zr-based analogue Zr-bptc with respect to overall connectivity and pore structure. However, the subtle difference in their structures lead to their distinct adsorption behaviors. One noticeable difference between them is that the framework of the Y-MOFs are anionic while the Zr-MOFs are neutral. To evaluate how the balancing cations in Y-MOFs may influence their pore apertures and contribute to their adsorption properties, we performed gas adsorption measurements on Y-abtc sample activated at different temperatures. The aforementioned adsorption measurements were performed on Y-abtc activated at 200 °C (Figure S15). ^{1}H NMR spectrum of the digested MOF sample indicates the dimethylammonium cations remain intact in the activated sample (Figure S16). On the other hand, Y-abtc activated at 300 °C shows enhanced adsorption capacity and kinetics toward propylene, compared to that of the sample activated at 200 °C (Figure S17), with propylene adsorbed amount of 3.5 mmol g^{-1} (v.s. 2.0 mmol g^{-1} if activated at 200 °C) at 25 °C and 1 bar. Adsorption rate measurements show the adsorption of propylene reach equilibrium within 10 and 4 minutes at 25 and 80 °C, respectively. In addition, upon activation at 300 °C, Y-abtc can adsorb a substantial amount of propane, through the diffusion rate is relatively slow. These results suggest that the increased activation temperature has noticeably enlarged the pore aperture of Y-abtc. To further confirm this hypothesis, CO_2 adsorption experiments at 195 K were carried out on Y-abtc samples activated at 200 and 300 °C. As expected, the sample activated at 300 °C adsorbs more CO_2 under saturation (**Figure 6**). Pore size distribution analysis confirms its enlarged pore size (4.93 Å) compared to that of the sample activated at 200 °C (4.72 Å). More evidently, the peak associated to dimethylammonium disappears on the ^{1}H NMR spectrum of the sample activated at 300 °C (Figure S16), indicating the decomposition of the organic cation. TG-MS measurement indicates that upon heating to 300 °C the material releases a molecular with a molecular mass of 45, which could be attributed to dimethylamine (Figure S18). This suggests the decomposition of dimethylammonium cation results in the formation of dimethylamine leaving proton (H^+) acting as balancing cation. This explains the observed enlarged pore aperture and its adsorption behavior toward

This article is protected by copyright. All rights reserved.

propylene and propane. CO_2 adsorption results and pore size distribution analysis on Y-bptc suggest a similar trend. This is interesting and noteworthy as ionic MOF frameworks are quite common and making use of the balancing ionic species as a pore size regulator can potentially be an effective way to develop adsorbents with optimal adsorption/separation performance.

Efficient separation of industrially relevant hydrocarbon mixtures by porous solids could potentially reduce the associated high energy cost, but remains challenging as it has stringent requirements for the adsorbents with respect to their adsorption/separation performance, stability, cost, to name a few. The development of inorganic adsorbents (e.g. zeolites) has led to great advancement of adsorptive separation technology and some excellent candidates have already been implemented for separations in industry. However, due to their limited structure diversity and lack of tunability, the search for novel adsorbents that can address such limitations is much needed and is indeed ongoing. Metal-organic frameworks are advantageous for molecular separation as they offer tremendous tunability in terms of structure, porosity, and functionality. Widely used strategies for tuning the pore structure and functionality of MOFs include reticular expansion/shrinkage by ligand design, pre-synthetic ligand functionalization, and post-synthetic functionalization of organic ligands or metal centers, to mention but a few. In this work, in addition to topologically directed framework expansion/shrinkage, we apply the strategy of SBU replacement to further tune the pore structure and make use of the balancing cations as pore size regulators to achieve optimal pore dimension for targeted hydrocarbon separation. The tailor-made Y-abtc displays efficient separation of propane and propylene through selective molecular exclusion. Moreover, it features high stability and scalable synthesis, rendering it a promising candidate for industrial implementation.

Experimental Section

Synthesis of Y-bptc: $Y(NO_3)_3{\cdot}6H_2O$ (38.3 mg, 0.1 mmol) and 2-fluorobenzoic acid (1.0 g, 4.1 mmol) were dissolved DMF/H_2O (5/2 mL) in a 20 mL glass vial and H_4bptc (16.5 mg, 0.05 mmol) was added to the solution. The mixture was solicated for 5 minutes before being placed in 120 °C oven for 3 days. Colorless cubic crystals were obtained by filtration. The crystals were washed by DMF (3 × 5 mL) and then immersed in 5 mL acetone for one week during which the solvent was replaced twice a day. The solvent-exchanged sample was dried at 200 °C under vacuum to yield activated sample. 50× scaled up synthesis resulted in materials with similar crystallinity.

Synthesis of Y-abtc: $Y(NO_3)_3{\cdot}6H_2O$ (38.3 mg, 0.1 mmol) and 2-fluorobenzoic acid (1.5 g, 6 mmol) were dissolved DMF/H_2O (5/2 mL) in a 20 mL glass vial and H_4abtc (17.5 mg, 0.05 mmol) was added to the solution. The mixture was solicated for 5 minutes before being placed in 120 °C oven for 3 days. Orange cubic crystals were obtained by filtration. The crystals were washed by DMF (3 × 5 mL)

This article is protected by copyright. All rights reserved.

Author Manuscript

and then immersed in 5 mL methanol for one week during which the solvent was replaced twice a day. The solvent-exchanged sample was dried at 200 or 300 °C under vacuum to yield activated sample. 50× scaled up synthesis resulted in material with similar crystallinity.

Crystal data for Y-bptc: Cubic crystal system, space group *Im-3*, *a* = 25.0883(6) Å, V = 15791.15(65) $Å^3$, Z = 8. ρ_{calc} = 1.46718 $g \cdot cm^{-3}$. CCDC No: 1853121.

Crystal data for Y-abtc: Trigonal crystal system, space group *R-3c*, *a* = 18.0682(7) Å, *c* = 45.3244(2) Å, V = 12814(1) $Å^3$, Z = 8. ρ_{calc} = 1.457(3) $g \cdot cm^{-3}$, $\mu(Cu\text{-}K_\alpha)$ =59.5(2) cm^{-1}. R_p and R_{wp} = 0.0754 and, 0.1022 for 5001 data collected in the 5–105° 2θ range. R_{Bragg} = 2.218. CCDC No.: 1856158.

[CCDC 1853121 and 1856158 contain the supplementary crystallographic data for this paper. These data can be obtained free of charge from The Cambridge Crystallographic Data Centre via www.ccdc.cam.ac.uk/data_request/cif.]

Supporting Information

Supporting Information is available from the Wiley Online Library or from the author.

Acknowledgements

We would like to thank the financial support from the Materials Sciences and Engineering Division, Office of Basic Research Energy Sciences of the U.S. Department of Energy through Grant No. DE-FG02-08ER-46491 for the synthesis, characterization and single-component adsorption work. Y.H. acknowledges the KAUST CCF fund for the breakthrough experiments. The RU team would also like to acknowledge Micromeritics Instrument Corp. for the award of a 3Flex system through its Instrument Grant program. V.C thanks the University of Milan for partial funding through the Development Plan of Athenaeum grant.

Author Manuscript

This article is protected by copyright. All rights reserved.

Received: ((will be filled in by the editorial staff))
Revised: ((will be filled in by the editorial staff))
Published online: ((will be filled in by the editorial staff))

Author Manuscript

References

[1] D. S. Sholl, R. P. Lively, *Nature* **2016**, *532*, 435.

[2] J. Padin, S. U. Rege, R. T. Yang, L. S. Cheng, *Chem. Eng. Sci.* **2000**, *55*, 4525.

[3] V. F. D. Martins, A. M. Ribeiro, M. G. Plaza, J. C. Santos, J. M. Loureiro, A. F. P. Ferreira, A. E. Rodrigues, *J. Chromatogr. A* **2015**, *1423*, 136.

[4] S. U. Rege, R. T. Yang, *Chem. Eng. Sci.* **2002**, *57*, 1139.

[5] C. A. Grande, A. E. Rodrigues, *Ind. Eng. Chem. Res.* **2001**, *40*, 1686.

[6] F. A. Da Silva, A. E. Rodrigues, *Ind. Eng. Chem. Res.* **1999**, *38*, 2051.

[7] M. Khalighi, Y. F. Chen, S. Farooq, I. A. Karimi, J. W. Jiang, *Ind. Eng. Chem. Res.* **2013**, *52*, 3877.

[8] X. Ma, S. Williams, X. Wei, J. Kniep, Y. S. Lin, *Ind. Eng. Chem. Res.* **2015**, *54*, 9824.

[9] H. Wang, W. P. Lustig, J. Li, *Chem. Soc. Rev.* **2018**.

[10] H. Furukawa, K. E. Cordova, M. O'Keeffe, O. M. Yaghi, *Science* **2013**, *341*.

[11] O. M. Yaghi, M. O'Keeffe, N. W. Ockwig, H. K. Chae, M. Eddaoudi, J. Kim, *Nature* **2003**, *423*, 705.

[12] H. Wang, W. P. Lustig, J. Li, *Chem. Soc. Rev.* **2018**, *47*, 4729.

[13] L. Bin, W. Hailong, C. Banglin, *Chem. - Asian J.* **2014**, *9*, 1474.

[14] K. Adil, Y. Belmabkhout, R. S. Pillai, A. Cadiau, P. M. Bhatt, A. H. Assen, G. Maurin, M. Eddaoudi, *Chem. Soc. Rev.* **2017**, *46*, 3402.

[15] A. Cadiau, K. Adil, P. M. Bhatt, Y. Belmabkhout, M. Eddaoudi, *Science* **2016**, *353*, 137.

[16] H. Wang, X. Dong, E. Velasco, D. H. Olson, Y. Han, J. Li, *Energy Environ. Sci* **2018**, *11*, 1226.

[17] B. Li, X. Cui, D. O'Nolan, H.-M. Wen, M. Jiang, R. Krishna, H. Wu, R.-B. Lin, Y.-S. Chen, D. Yuan, H. Xing, W. Zhou, Q. Ren, G. Qian, M. J. Zaworotko, B. Chen, *Adv. Mater.* **2017**, *29*, 1704210.

This article is protected by copyright. All rights reserved.

[18] S. J. Geier, J. A. Mason, E. D. Bloch, W. L. Queen, M. R. Hudson, C. M. Brown, J. R. Long, *Chem. Sci.* **2013**, *4*, 2054.

[19] E. D. Bloch, W. L. Queen, R. Krishna, J. M. Zadrozny, C. M. Brown, J. R. Long, *Science* **2012**, *335*, 1606.

[20] A. van Miltenburg, J. Gascon, W. Zhu, F. Kapteijn, J. A. Moulijn, *Adsorption* **2008**, *14*, 309.

[21] C. A. Grande, N. Firpo, E. Basaldella, A. E. Rodrigues, *Adsorption* **2005**, *11*, 775.

[22] J. Peng, H. Wang, D. H. Olson, Z. Li, J. Li, *Chem. Commun.* **2017**, *53*, 9332.

[23] K. Li, D. H. Olson, J. Seidel, T. J. Emge, H. Gong, H. Zeng, J. Li, *J. Am. Chem. Soc.* **2009**, *131*, 10368.

[24] C. Y. Lee, Y.-S. Bae, N. C. Jeong, O. K. Farha, A. A. Sarjeant, C. L. Stern, P. Nickias, R. Q. Snurr, J. T. Hupp, S. T. Nguyen, *J. Am. Chem. Soc.* **2011**, *133*, 5228.

[25] Y. Wang, D. Zhao, *Cryst. Growth Des.* **2017**, *17*, 2291.

[26] C. A. Grande, A. E. Rodrigues, *Chem. Eng. Res. Des.* **2004**, *82*, 1604.

[27] M. Khalighi, I. A. Karimi, S. Farooq, *Ind. Eng. Chem. Res.* **2014**, *53*, 16973.

[28] D.-X. Xue, A. Cadiau, L. J. Weselinski, H. Jiang, P. M. Bhatt, A. Shkurenko, L. Wojtas, C. Zhijie, Y. Belmabkhout, K. Adil, M. Eddaoudi, *Chem. Commun.* **2018**, *54*, 6404.

[29] H. Wang, X. Dong, J. Lin, S. J. Teat, S. Jensen, J. Cure, E. V. Alexandrov, Q. Xia, K. Tan, Q. Wang, D. H. Olson, D. M. Proserpio, Y. J. Chabal, T. Thonhauser, J. Sun, Y. Han, J. Li, *Nat. Commun.* **2018**, *9*, 1745.

[30] Y. Bai, Y. Dou, L.-H. Xie, W. Rutledge, J.-R. Li, H.-C. Zhou, *Chem. Soc. Rev.* **2016**, *45*, 2327.

[31] D.-X. Xue, Y. Belmabkhout, O. Shekhah, H. Jiang, K. Adil, A. J. Cairns, M. Eddaoudi, *J. Am. Chem. Soc.* **2015**, *137*, 5034.

[32] V. Guillerm, Ł. J. Weseliński, Y. Belmabkhout, A. J. Cairns, V. D'Elia, Ł. Wojtas, K. Adil, M. Eddaoudi, *Nat. Chem.* **2014**, *6*, 673.

[33] R. Luebke, Y. Belmabkhout, Ł. J. Weseliński, A. J. Cairns, M. Alkordi, G. Norton, Ł. Wojtas, K. Adil, M. Eddaoudi, *Chem. Sci.* **2015**, *6*, 4095.

[34] A. A. H., B. Youssef, A. Karim, B. P. M., X. Dong‐Xu, J. Hao, E. Mohamed, *Angew. Chem. Intl. Ed.* **2015**, *54*, 14353.

[35] R. Luebke, Y. Belmabkhout, L. J. Weselinski, A. J. Cairns, M. Alkordi, G. Norton, L. Wojtas, K. Adil, M. Eddaoudi, *Chem. Sci.* **2015**, *6*, 4095.

Author Manuscript

This article is protected by copyright. All rights reserved.

[36] C. A. A., *J. Appl. Crystallogr.* **2003**, *36*, 86.

[37] V. A. Blatov, A. P. Shevchenko, D. M. Proserpio, *Cryst. Growth Des.* **2014**, *14*, 3576.

[38] C. Bonneau, M. O'Keeffe, D. M. Proserpio, V. A. Blatov, S. R. Batten, S. A. Bourne, M. S. Lah, J.-G. Eon, S. T. Hyde, S. B. Wiggin, L. Öhrström, *Cryst. Growth Des.* **2018**, *18*, 3411.

[39] B. Demir, M. G. Ahunbay, *Micro. Meso. Mater.* **2014**, *198*, 185.

[40] J.-R. Li, R. J. Kuppler, H.-C. Zhou, *Chem. Soc. Rev.* **2009**, *38*, 1477.

Author Manuscript

This article is protected by copyright. All rights reserved.

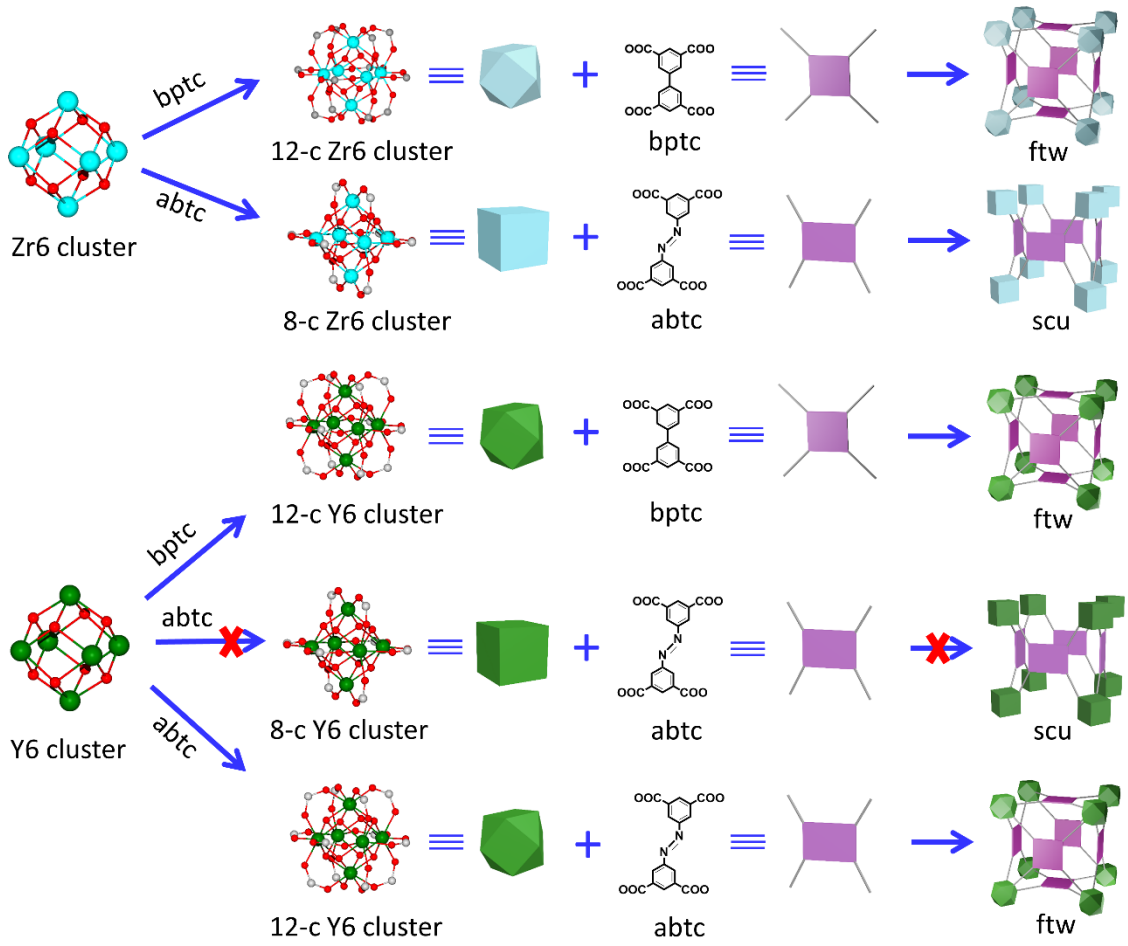

Figure 1. Topology analysis of MOFs built on Zr6/Y6 clusters and two tetratopic linkers. Zr-bptc and Zr-abtc show different connectivity and topology due to the difference of the aspect ratio of organic linkers. Y-bptc and Y-abtc feature similar connectivity and topology to that of Zr-bptc. Hydrogen atoms are omitted for clarity.

Author

This article is protected by copyright. All rights reserved.

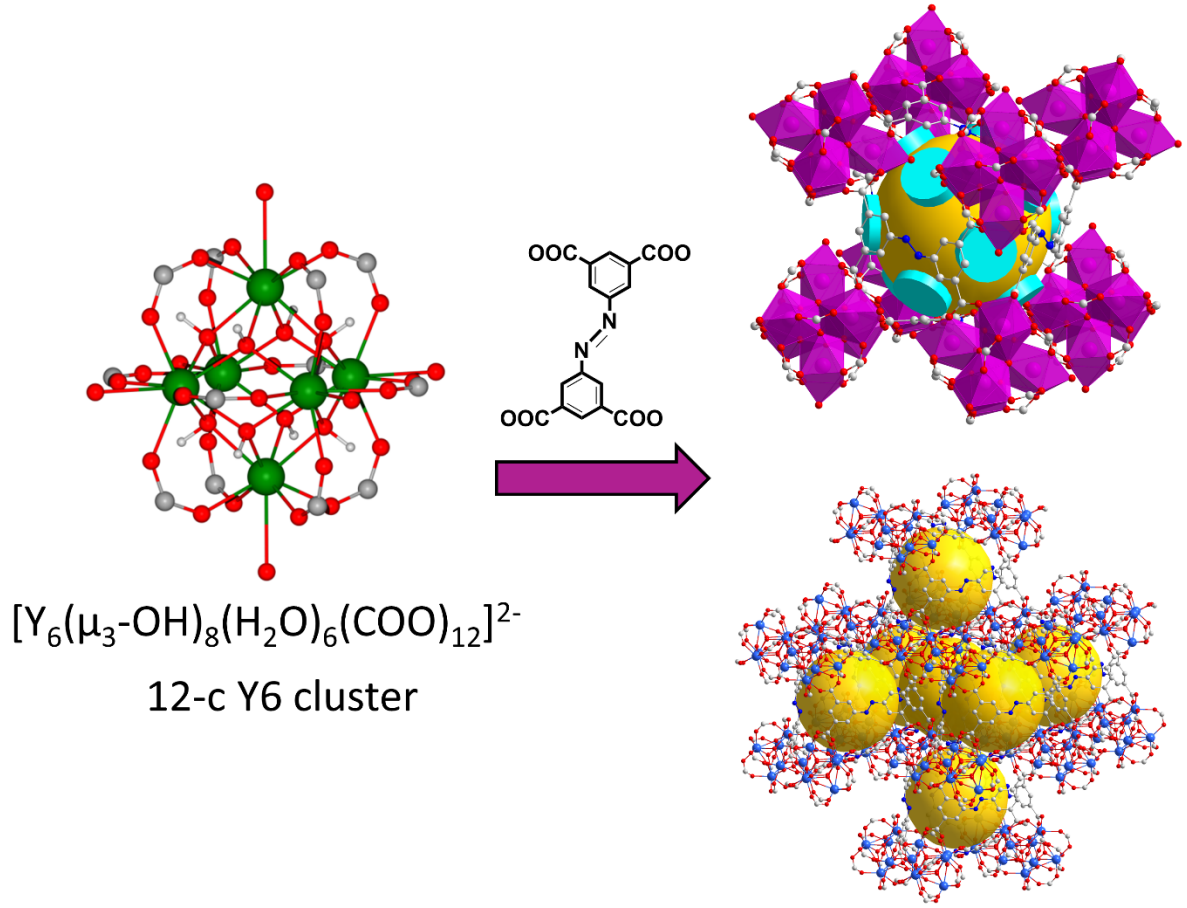

Figure 2. Crystal structure of Y-abtc. Y-abtc is built on 12-connected hexanuclear SBU, forming cage-like pores interconnected by small windows.

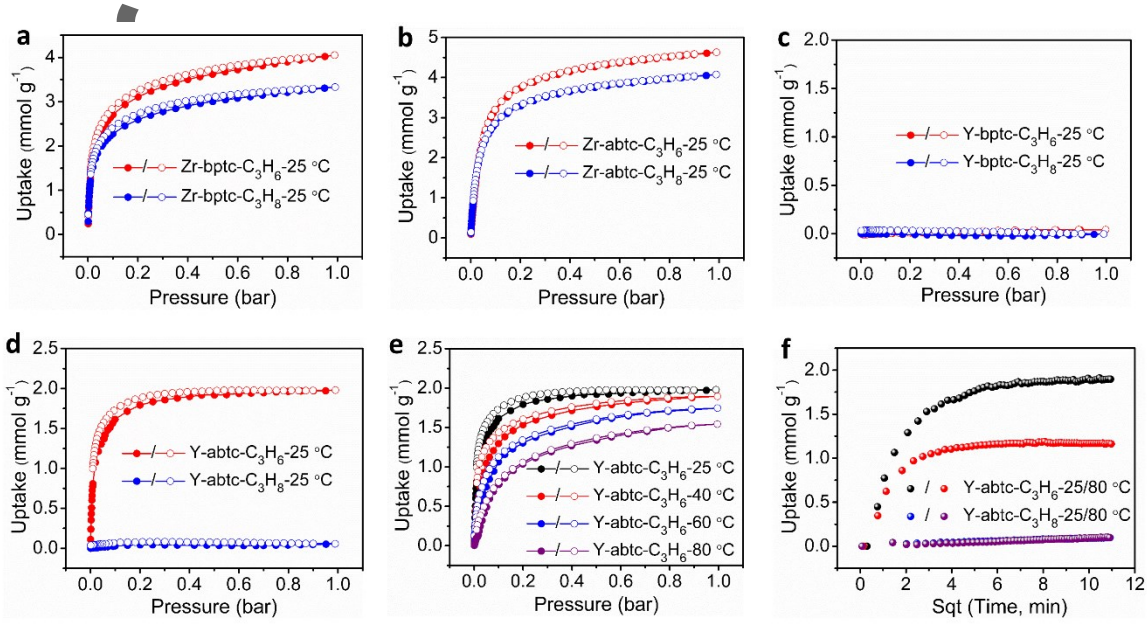

This article is protected by copyright. All rights reserved.

Figure 3. Single-component adsorption results of propane and propylene. Adsorption-desorption isotherms of propane and propylene at 25 °C for a) Zr-bptc, b) Zr-abtc, c) Y-bptc, and d) Y-abtc. e) Propylene adsorption isotherms for Y-abtc at 25, 40, 60, and 80 °C. f) Adsorption rates of propane and propylene on Y-abtc at 25 and 80 °C, with a partial pressure of 0.8 bar.

Author Manuscript

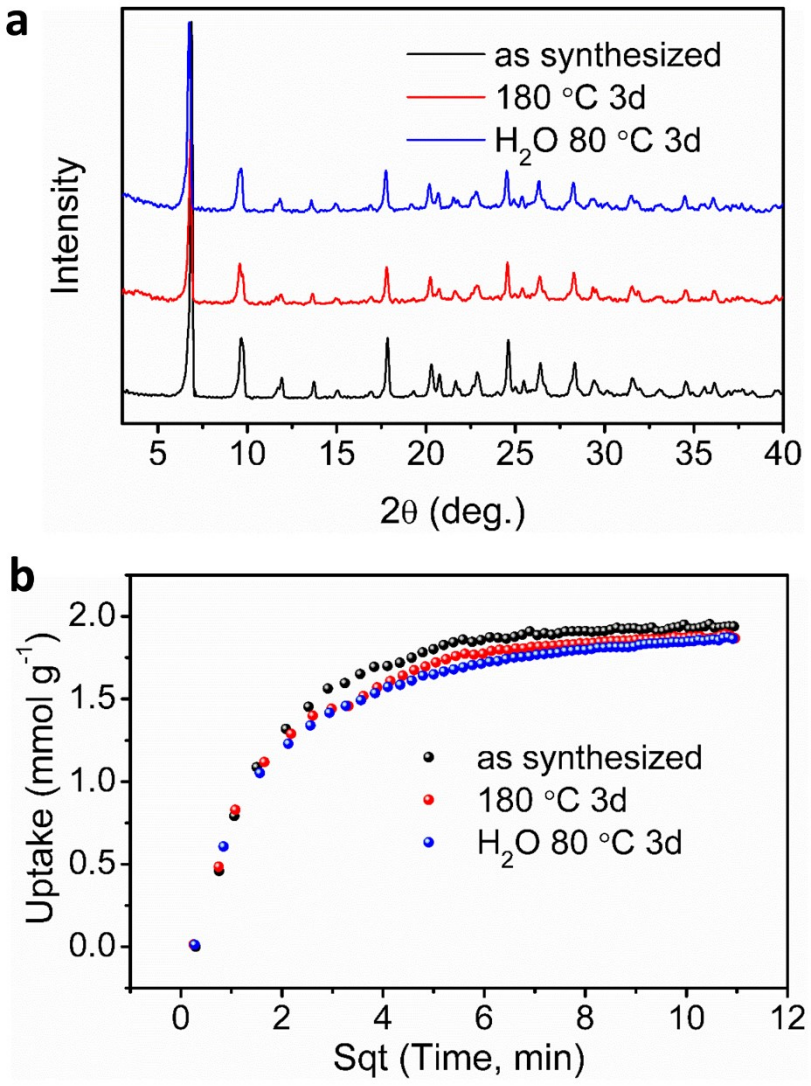

Figure 4. Stability test for Y-abtc. a) Powder X-ray diffraction patterns and b) propylene adsorption for as synthesized Y-abtc and after thermal and hydrothermal treatments.

This article is protected by copyright. All rights reserved.

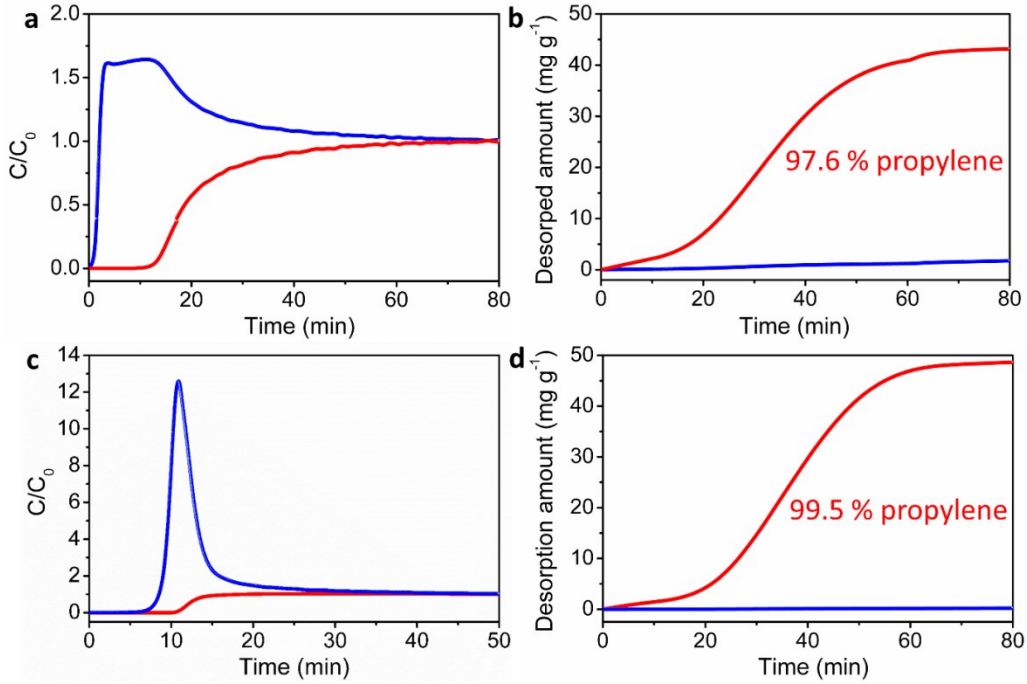

Figure 5. Multicomponent column breakthrough results for Y-abtc at 25 °C. a) Breakthrough curve and b) desorption curve for an equimolar mixture of propane and propylene. c) Breakthrough curve and d) desorption curve for a mixture of propane/propylene with a feed ratio of 5/95. Color scheme: red: propylene, blue: propane.

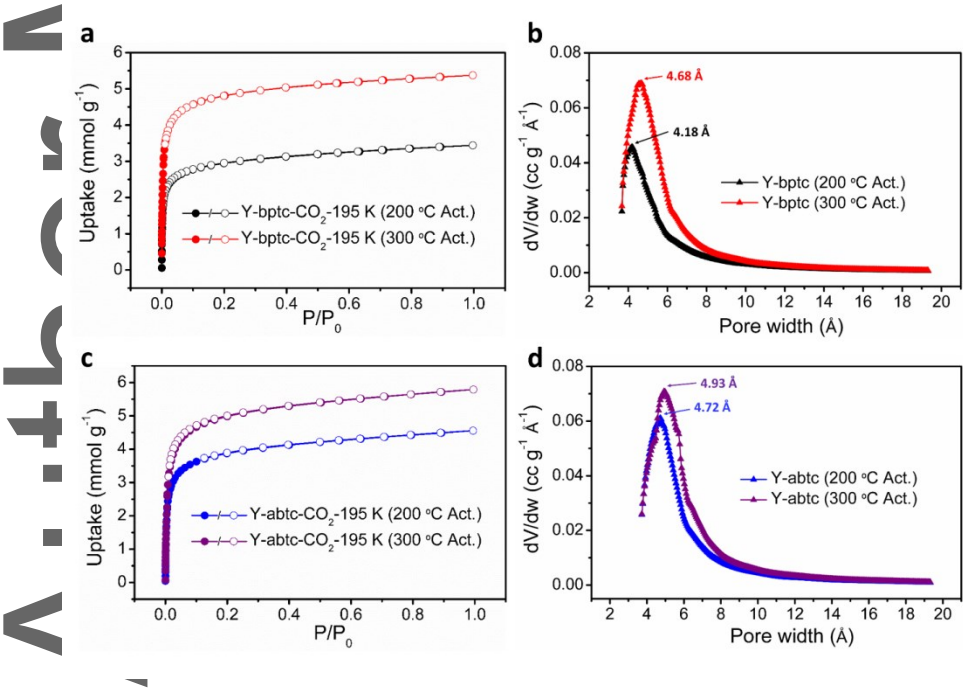

This article is protected by copyright. All rights reserved.

Figure 6. a) Adsorption-desorption isotherm of CO_2 at 195 K on Y-bptc activated at 200 and 300 °C and b) the corresponding pore size distribution. c) Adsorption-desorption isotherm of CO_2 at 195 K on Y-abtc activated at 200 and 300 °C and d) the corresponding pore size distribution.

Author Manuscript

This article is protected by copyright. All rights reserved.

Author Manuscript

A tailor-made microporous metal-organic framework designed through a topologically guided SBU replacement strategy exhibits the highest selectivity for fast and efficient separation of propane and propylene via size exclusion adsorption mechanism. This material, with excellent thermal and hydrothermal stability, facile and scalable synthesis, is capable of producing polymer-grade propylene (99.5%) from a typical propane/propylene mixture of cracking products.

metal-organic frameworks, adsorptive separation, olefin/paraffin separation, molecular sieving

Hao Wang, Xinglong Dong, Valentina Colombo, Qining Wang, Yanyao Liu, Wei Liu, Xin-Long Wang, Xiao-Ying Huang, Davide M. Proserpio, Angelo Sironi, Yu Han, and Jing Li*

Tailor-Made Microporous Metal-Organic Frameworks for the Full Separation of Propane from Propylene Through Selective Size Exclusion

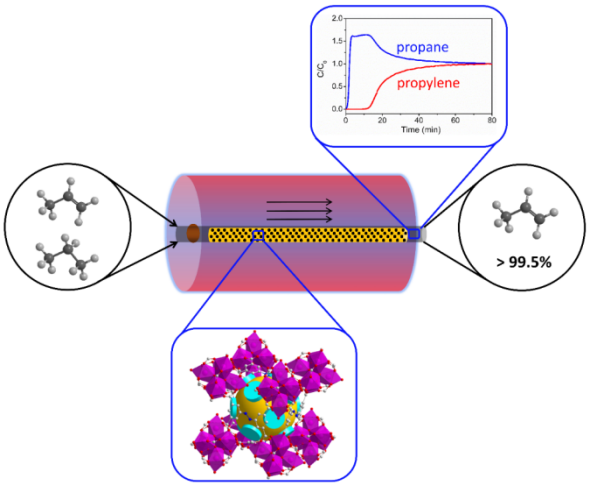

This article is protected by copyright. All rights reserved.